Article

Not peer-reviewed version

Evaluation of Superparamagnetic Fe3O4-Ag Decorated Nanoparticles: Cytotoxicity Studies in Human Fibroblasts (HFF-1) and Breast Cancer Cells (MCF-7)

Álvaro de Jesús Ruíz-Baltazar *, Simón Yobanny Reyes-López, Néstor Méndez-Lozano, Karla Juarez-Moreno *

Posted Date: 1 July 2024

doi: 10.20944/preprints202407.0009.v1

Keywords: superparamagnetic nanoparticles; cytotoxicity, biocompatibility; biomedical applications

Article

Evaluation of Superparamagnetic Fe_3O_4-Ag Decorated Nanoparticles: Cytotoxicity Studies in Human Fibroblasts (HFF-1) and Breast Cancer Cells (MCF-7)

Álvaro de Jesús Ruíz-Baltazar [1,2,*] Simón Yobanny Reyes-López [2], Néstor Mendez-Lozano [3] and Karla Juarez-Moreno [4,*]

[1] CONAHCYT-Centro de Física Aplicada y Tecnología Avanzada, Universidad Nacional Autónoma de México, Boulevard Juriquilla 3001, Santiago de Querétaro, Qro., 76230, México.
[2] Instituto de Ciencias Biomédicas, Departamento de Ciencias Químico-Biológicas, Universidad Autónoma de Ciudad Juárez, Anillo Envolvente del Pronaf y Estocolmo s/n, Zona Pronaf, Ciudad Juárez 32310, Mexico
[3] Campus Querétaro, Universidad del Valle de México, Blvd. Juriquilla no. 1000 A. Del. Santa Rosa Jáuregui, Querétaro 76230
[4] Centro de Física Aplicada y Tecnología Avanzada, Universidad Nacional Autónoma de México, Boulevard Juriquilla 3001, Santiago de Querétaro, Qro., 76230, México
* Correspondence: aruizbaltazar@fata.unam.mx and kjuarez@fata.unam.mx

Abstract: This study investigates the cytotoxicity profile of superparamagnetic Fe3O4-Ag decorated nanoparticles against human fibroblasts (HFF-1) and breast cancer cells (MCF-7). The nanoparticles underwent comprehensive characterization employing scanning electron microscopy (SEM), X-ray diffraction (XRD) analysis, X-ray photoelectron spectroscopy (XPS), and magnetic assays including hysteresis curves and zero-field-cooled (ZFC) plots. The nanoparticles exhibited superparamagnetic behavior as evidenced by magnetic studies. Cytotoxicity assays demonstrated that both HFF-1 and MCF-7 cells maintained nearly 100% viability upon nanoparticle exposure, underscoring the outstanding biocompatibility of Fe3O4/Ag decorated nanoparticles and suggesting their potential utility in biomedical applications such as drug delivery and magnetic targeting. Furthermore, the study analyzed the cytotoxic effects of Fe3O4 and Fe3O4-Ag decorated nanoparticles to evaluate their biocompatibility and therapeutic efficacy. Results showed that neither type of nanoparticle significantly reduced cell viability in HFF-1 fibroblasts, indicating non-cytotoxicity at the tested concentrations. Similarly, MCF-7 breast cancer cells did not exhibit a significant change in viability when exposed to different nanoparticle concentrations, highlighting the compatibility of these nanoparticles with both healthy and cancerous cells. Additionally, the production of reactive oxygen species (ROS) by the nanoparticles was examined to assess their therapeutic potential. Higher concentrations of Fe3O4-Ag nanoparticles decreased ROS production in both HFF-1 and MCF-7 cells, while Fe3O4 nanoparticles were more effective in generating ROS. This differential response suggests that Fe3O4-Ag nanoparticles might modulate oxidative stress more effectively, beneficial for anticancer strategies due to cancer cells' susceptibility to ROS-induced damage. These findings contribute to understanding nanoparticle interactions with cellular oxidative mechanisms, crucial for developing safe and effective nanoparticle-based therapies. This investigation advances our understanding of nanostructured materials in biological settings and highlights their promising prospects in biomedicine.

Keywords: superparamagnetic nanoparticles; cytotoxicity; biocompatibility; biomedical applications

1. Introduction

 doi:10.20944/preprints202407.0009.v1

Nanotechnology has emerged as a promising field in the realm of biomedical applications, offering innovative solutions for targeted drug delivery, cancer diagnostics, and therapeutic interventions[1–3]. Among the diverse nanomaterials available, superparamagnetic iron oxide nanoparticles (SPIONs) have garnered significant attention due to their exceptional physicochemical properties, including their high surface area, biocompatibility, and magnetic responsiveness[4,5]. These unique characteristics have led to the exploration of iron oxide nanoparticles, particularly Fe3O4, in various biomedical applications, such as magnetic resonance imaging (MRI), hyperthermia-based cancer treatment, and drug delivery[6,7].

The synthesis and functionalization of Fe3O4 nanoparticles have been extensively investigated, with researchers exploring different strategies to enhance their stability, biocompatibility, and targeting capabilities[8,9]. One approach that has shown promise is the decoration of Fe3O4 nanoparticles with silver (Ag) to create Fe3O4-Ag structures[10]. The addition of silver can potentially improve the antibacterial properties and electrical conductivity of the nanoparticles, making them attractive for a wide range of biomedical applications[11,12]. Another application of the Fe3O4-Ag nanoparticles is in the field of cancer therapy[13,14]. The enhanced magnetic and plasmonic properties of the decorated nanoparticles can be leveraged for targeted drug delivery, photothermal therapy, and magnetic hyperthermia. On the one hand, the magnetic properties allow for the nanoparticles to be guided to the tumor site using an external magnetic field[15–17]. On the other hand, the silver coating can potentially enhance the cytotoxic effects on cancer cells through generation of reactive oxygen species and disruption of cellular processes[18].

To fully harness the potential of Fe3O4-Ag decorated nanoparticles in biomedical applications, it is crucial to understand their cytotoxicity and biocompatibility in relevant cell lines. Human fibroblasts (HFF-1) and breast cancer cells (MCF-7) serve as important model systems for evaluating the biological impact of these nanoparticles, as they represent crucial components of the human body -healthy cells and cancer cells, respectively[19–21].

Regarding to the obtention of these magnetoplasmonic structures, the synthesis of Fe3O4-Ag decorated nanoparticles can be achieved through various chemical and biological methods[10]. Typically, the core Fe3O4 nanoparticles are first prepared, followed by the deposition of silver onto the surface. several synthesis method of Fe3O4-Ag nanoparticles have been reported, such as co-precipitation, thermal decomposition, microemulsion, and green synthesis approaches using plant extracts or microbial agents[22–24]. Recently, green synthesis methods have gained attention due to their eco-friendly nature and the potential to produce biocompatible nanoparticles[25,26]. For example the use of deep eutectic solvents as reducing and stabilizing agents in the synthesis of Fe3O4-Ag nanoparticles has been reported[27,28]. However, the Chemical reduction is one of the most widely used methods for the synthesis of these nanostructures, as it allows for precise control over the size, morphology, and composition of the nanoparticles [22,29,30]. The formation of the silver shell or decorated on the Fe3O4 core can be achieved through the reduction of silver nitrate (AgNO3) in the presence of a reducing agent, such as sodium borohydride or ascorbic acid[31]. The resulting Fe3O4-Ag nanoparticles can be further functionalized with various biomolecules, polymers, or drug compounds to enhance their biocompatibility, targeting, and therapeutic capabilities[32,33].

In this sense, the evaluation of the cytotoxic effects of Fe3O4-Ag decorated nanoparticles is an important aspect of their biomedical application. Human fibroblasts (HFF-1) and breast cancer cells (MCF-7) are commonly used as model cell lines to assess the biocompatibility and potential anticancer properties of nanoparticles.

Human fibroblasts, such as HFF-1 cells, represent a non-cancerous cell line that is often employed to determine the overall biocompatibility and safety of nanoparticles[34]. The evaluation of the cytotoxicity of Fe3O4-Ag nanoparticles in HFF-1 cells can provide insights into their potential toxic effects on healthy cells, which is crucial for their development as safe and effective biomedical agents.

On the other hand, breast cancer cell lines, such as MCF-7, are used to assess the anticancer potential of Fe3O4-Ag nanoparticles. The ability of these nanoparticles to selectively induce

 doi:10.20944/preprints202407.0009.v1

cytotoxicity in cancer cells while sparing healthy cells is a desirable characteristic for their application in cancer therapy[27,31].

The cytotoxicity studies typically involve exposing the cell lines to varying concentrations of the Fe3O4-Ag nanoparticles and evaluating their effects on cell viability, proliferation, and morphology using various assays, such as MTT, LDH, or live/dead staining. These studies can elucidate the dose-dependent cytotoxic responses of the nanoparticles and provide valuable insights into their biocompatibility and potential therapeutic efficacy [14,35].

Therefore, a comprehensive evaluation of the cytotoxicity of these novel Fe3O4-Ag-decorated nanoparticles on relevant cell lines is vital to evaluate their potential for biomedical applications. This study is designed to investigate the cytotoxic effects of Fe3O4-Ag nanoparticles on human fibroblasts (HFF-1) and breast cancer cells (MCF-7), providing crucial information on their biocompatibility and potential therapeutic applications.

2. Materials and Methods

2.1. Synthesis of Fe3O4-Ag Decorated Nanoparticles:

The synthesis of Fe3O4 nanostructures commenced by utilizing FeCl3·6H2O as a precursor at a concentration of 0.01 M. Reduction of Fe3+ ions was achieved using a solution of NaBH4 (0.02 M), with polyvinylpyrrolidone (PVP) serving as a stabilizing surfactant at a concentration of 0.1 M. Deionized water was employed as the colloidal medium. The PVP/FeCl3·6H2O ratio was maintained at 50, a parameter known to promote the formation of magnetite nanostructures [21]. Following the reduction of Fe3+ ions, an oxidative etching process was employed to facilitate the formation of magnetite, a mechanism established in prior studies for Fe3O4 nanostructure synthesis [21]. Importantly, all experiments were conducted at room temperature under a constant hydrogen potential (pH = 11). The proposed reduction process involves the initial decomposition of NaBH4, generating hydrogen, which in turn facilitates the reduction of Fe3+ ions, leading to the formation of iron nanoparticles.

Subsequently, to the preformed Fe3O4 nanoparticles, a solution of AgNO3 (50 mM, 20 mL) was added, and the mixture was agitated at room temperature. Following this, a solution of NaBH4 (2 mM, 5 mL) was promptly added, resulting in the formation of silver nuclei on the Fe3O4 particles. This process was visually discernible by a change in coloration from black to dark gray, culminating in the synthesis of Fe3O4-Ag decorated nanoparticles.

2.2. Chemical and Structural Characterization of Fe3O4-Ag Decorated:

The Fe3O4-Ag decorated nanoparticles underwent comprehensive characterization using scanning electron microscopy (SEM) with a Hitachi model 8230 microscope. Various electron detection techniques were employed to obtain a thorough understanding of the morphology and chemical composition. High-resolution images acquired through High-Angle Secondary Electron (SE-HA) microscopy highlighted the presence of Fe3O4 and Ag phases, while Secondary Electron (SE(U)) imaging provided detailed surface topography. High-Angle Backscattered Electron (HA(T)) analyses discerned chemical element distribution, exploiting the technique's sensitivity to atomic number. Composite images revealing both morphology and elemental composition were generated using SE+HA+OFF by combining secondary and backscattered electron detectors. Additionally, chemical analysis via Energy-Dispersive X-ray Spectroscopy (EDS) mapped the distribution of iron (Fe), oxygen (O), and silver (Ag) in the nanoparticles, confirming the presence and uniformity of Ag decoration on the Fe3O4 surface. SEM operational parameters included a magnification of x500k, a working distance of 3.7 mm, and an acceleration voltage of 3.0 kV, ensuring precise and accurate results from EDS mappings conducted in representative areas.

Furthermore, the magnetic nanoparticle characterization involved utilizing an X-ray diffractometer (Rigaku Ultima IV) equipped with Cu-Kα radiation, employing parallel-beam geometry and 2θ scans spanning from 15 to 80°. Magnetic analyses were conducted using a vibrating sample magnetometer (VSM) at 300 K.

 doi:10.20944/preprints202407.0009.v1

2.3. *Analysis of Cytotoxicity*

2.3.1. Cell Lines Culture

The human breast adenocarcinoma MCF-7 cells (ATCC-HTB-22) and Human Fibroblasts HFF-1 (SRC-1041) were acquired from the American Type Culture Collection (ATCC). These cells were cultivated at a temperature of 37◦C with 5% of CO_2 in Dulbecco's Modified Eagle's Medium (DMEM), supplemented with 10% Fetal Bovine Serum (FBS, BenchMark, Geminis Bio Products), 1% Penicillin-Streptomycin (Sigma-Aldrich), 1% L-glutamine, and 2 g/L of sodium bicarbonate.

2.3.2. Cytotoxicity Assay by MTT reduction

The effect of Fe_3O_4 and Fe_3O_4-Ag decorated nanoparticles on cell viability was evaluated using the MTT reduction. MCF-7 and HFF-1 cells were seeded at a density of 10,000 cells per well in a 96-well plate and exposed to different concentrations of nanoparticles from 0.1 to 100 µg/mL. Cell viability was assessed by measuring the reduction of MTT, a tetrazolium compound, following the manufacturer's instructions. Tween at 1% in PBS served as the positive control, inducing complete cell death, while cells cultured in DMEM were the negative control. Experiments were conducted in triplicate, and absorbance readings were taken at 570 and 690 nm using a plate reader. Cell viability was calculated relative to the absorbance values of the positive control.

2.3.3. Measurement of Reactive Oxygen Species Production

To measure the production of reactive oxygen species (ROS), cells were seeded in a 48-well plate and exposed to several concentrations from 0.1 to 100 µg/mL of Fe_3O_4 or Fe_3O_4-Ag nanoparticles for 24 h. After exposure, cells were treated with 25 µM of 2',7'-dichlorofluorescein diacetate and incubated for 1 h at at 37°C with 5% CO_2. Then cells were washed and harvested before being analyzed using flow cytometry. ROS levels were assessed using the Bl-1 channel with specific excitation and emission wavelength s at 488 nm and 525, respectively. The level of endogenous ROS was determined for each cell line without any treatment. Experiments were conducted in triplicate across three independent trials, and flow cytometry data were acquired using an Attune NxT flow cytometry (Life Technologies, Carlsbad, California, USA) with 10,000 events (cells) recorded for each sample. Further data analysis was achieved using the Attune NxT acquisition software version 3.2.1. (Thermofisher).

2.3.4. Measurement of Nitrite Production by Macrophages

The Griess assay was employed to quantify nitrite production by macrophages following exposure to different concentrations of Fe_3O_4 or Fe_3O_4-Ag nanoparticles. In macrophages, nitrites result from the oxidation of nitric oxide in the modulation of inflammation and other physiological processes. RAW 264.7 macrophages were seeded in a 96-well plate at a density of 10,000 cells per well and cultured for 24 hours at 37°C and 5% CO_2. Different concentrations of Fe_3O_4 or Fe_3O_4-Ag nanoparticles from 0.1 to 100 µg/mL were added to the wells and further incubated for 24 hours under the same conditions. Subsequently, 20 µL of cell culture supernatant from each well was combined with 80 µL of 5 mM sodium nitroprusside in a new well, followed by incubation for 1 hour in darkness at 37°C and 5% CO_2. Next, the reaction mixture was treated with 100 µL of Griess reagent solution (0.1% sulfanilamide and 0.1% N-(1-naphthylethylenediamine)) and incubated at 25°C for 15 minutes in darkness. Absorbance was measured at 540 nm, and the values were compared against a standard curve generated using sodium nitrite concentrations ranging from 1.67 to 100 µM as reference reagents for nitrite production. Experiments were conducted independently in triplicate, three times over.

2.3.5. Hemocompatibility Assay

Human red blood cells were extracted from the peripheral blood of a healthy donor with normal cell morphology. The hemocompatibility assessment followed ISO 10993-4 standards. Blood was

 doi:10.20944/preprints202407.0009.v1

collected in sodium heparin-containing tubes (BD USA), red blood cells (RBCs) were isolated by centrifugation, then, cells were rinsed with 10 mL of 150 mM NaCl, followed by washes with 1x PBS. The RBCs were then diluted 1:50 in PBS, and 100 µL of the solution was placed into each well of a 96-well plate. Fe_3O_4 or Fe_3O_4-Ag nanoparticles were added at a 0.1 to 100 µg/mL concentration. After incubation for 1 hour at 37°C, samples were centrifuged at 10,000 rpm for 5 minutes. The absorbance of the supernatant was measured at 550 nm. The hemolysis percentage was calculated using the formula: Hemolysis (%) = (OD 550 nm sample - OD 550 nm negative control) / (OD 550 nm positive control - OD 550 nm negative control) * 100. PBS-treated RBCs served as the negative control, showing no hemolysis. RBCs treated with 0.1% Triton X-100 in PBS were the positive control, inducing 100% hemolysis. Background signal at 550 nm was subtracted for each experiment. According to ISO standards, acceptable hemolysis of RBCs is ≥5%.

2.3.6. Statistical Analysis

Statistical analysis was conducted through three independent experiments, each carried out in triplicates. The results were presented as mean ± standard deviation from three independent experiments. The data underwent analysis of variance (ANOVA) and subsequent Tukey's Multiple Comparison Test, facilitated by GraphPad Prism version 10 software. Statistical significance was determined at a threshold of $p<0.05$.

3. Results and Discussion

3.1. Scanning Electron Microscopy Analysis

Figure 1 presents scanning electron microscopy (SEM) images of the Fe3O4-Ag sample. These images provide insights into the morphology and elemental composition of the nanoparticles. Figure 1a) displays an SE-HA (High-Angle Secondary Electron) image captured using high-angle secondary electron detectors. This image reveals the nanoparticle topology, clearly indicating the presence of Fe3O4 and Ag phases. Figure 1b) depicts an SE(U) image, corroborating the presence of Fe3O4 and Ag. These images utilize secondary electron emission from the sample surface upon primary electron beam interaction, providing high-resolution surface topography details. Figure 1c) showcases an HA(T) (High-Angle Backscattered Electron) image, obtained using high-angle backscattered electron detectors, highlighting the formation of Fe3O4-Ag. Lastly, Figure 1d) illustrates an SE+HA+OFF image, indicating the simultaneous use of both secondary and backscattered electron detectors, with the secondary electron detector turned off. This combined imaging approach offers a comprehensive view of both surface morphology and elemental composition. All images were captured at x500k magnification, with a working distance of 3.7mm and an acceleration voltage of 3.0 kV. The SEM imaging results suggest the formation of a decorated Fe3O4-Ag structure, attributed to variations in the nucleation and growth rates of magnetite and silver structures. The successful synthesis of these decorated structures is evident from the captured images. This underscores the efficacy of the proposed methodology in fabricating such decorated structures.

 doi:10.20944/preprints202407.0009.v1

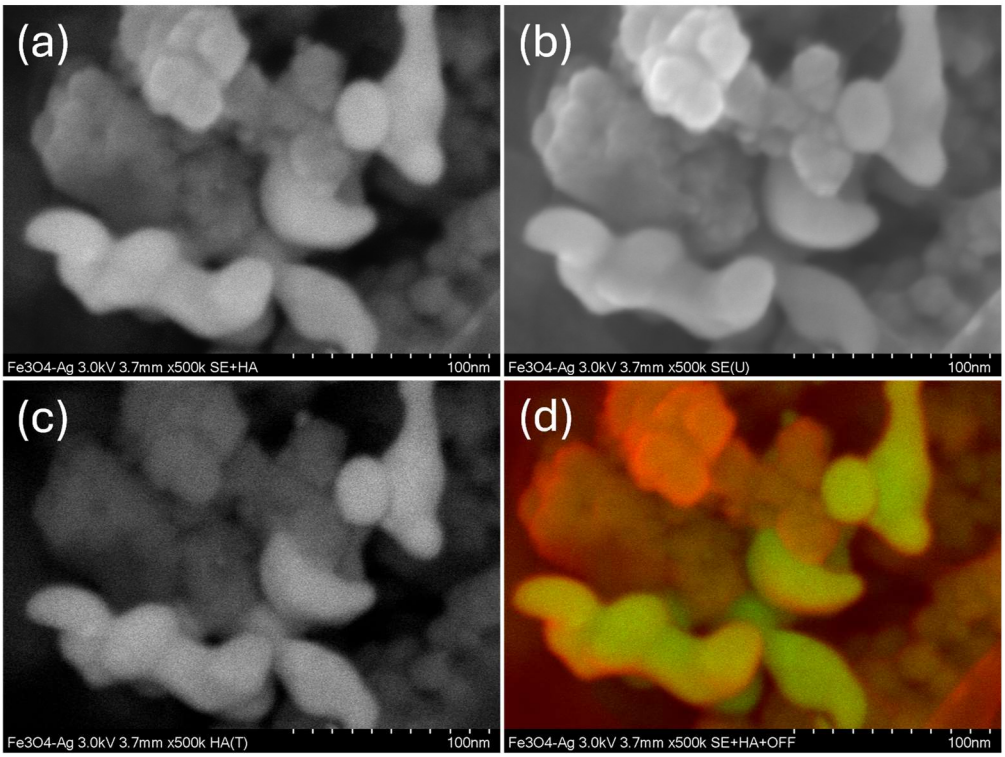

Figure 1. SEM micrographs depicting the Fe3O4-Ag nanoparticle sample. (a) SE-HA image showing nanoparticle topology and the presence of Fe3O4 and Ag phases. (b) SE(U) image confirming Fe3O4 and Ag presence, providing high-resolution surface details. (c) HA(T) image emphasizing Fe3O4-Ag formation. (d) SE+HA+OFF composite image displaying surface morphology and elemental composition. Magnification: x500k; Working distance: 3.7mm; Acceleration voltage: 3.0 kV.

The chemical analysis depicted in Figure 2 was conducted using Energy Dispersive X-ray Spectroscopy (EDS). In Figure 2a, the secondary electron (SE) image of the Fe3O4 configuration is presented. In Figure 2b, a mapping of the sample illustrates the distribution of silver (Ag) on the iron oxide structure, confirming the formation of the decorated Fe3O4-Ag structure. Subsequently, Figures 2c-e display elemental mappings of iron (Fe), oxygen (O), and silver (Ag) from the SE image of Fe3O4. Lastly, Figure 2(f) presents a chemical analysis of the Fe3O4 sample, confirming the predominant presence of elements such as Fe, O, and Ag. These results elucidate the chemical composition of the decorated nanoparticles, whose cytotoxic performance will be further investigated in this study.

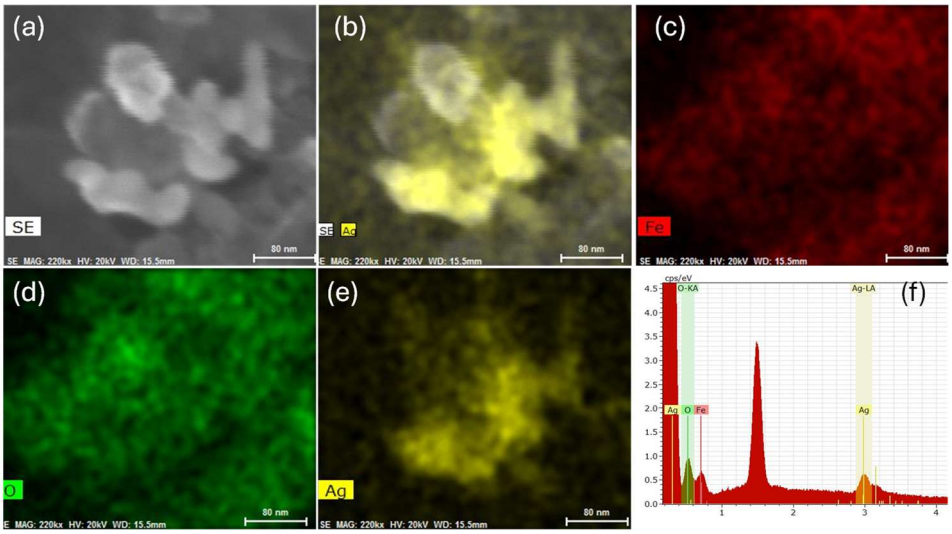

 doi:10.20944/preprints202407.0009.v1

Figure 2. Chemical Analysis of Fe3O4-Ag Decorated Nanoparticles. (a) SE image of Fe3O4. (b) Elemental mapping showing Ag distribution, confirming Fe3O4-Ag structure. Elemental mappings of Fe, O, and Ag from SE image of Fe3O4 are in (c-e). (f) Chemical analysis confirms Fe, O, and Ag composition.

3.2. X-ray Diffraction Analysis.

Additionally, structural characterization of the sample is essential to support the configuration of the obtained nanoparticles. X-ray diffraction (XRD) analysis was performed to elucidate the structure and composition of the synthesized nanoparticles.

The XRD pattern reveals the cubic FCC structure of silver (Ag), as evidenced by the characteristic peaks corresponding to the JCPDF # 87-0598, with a theoretical lattice parameter of 2.31 nm. Based on the observed intensities in the experimental X-ray pattern, the symmetry associated with the Fm3m space group and the spatial group of 325 were determined. This result confirms the presence of the Fe3O4 and Ag alloy, forming the synthesized nanoparticles. The subsequent evaluation of sample properties will be based on this confirmation.

Furthermore, the XRD pattern displays prominent peaks corresponding to the cubic structure of Fe3O4. Specifically, peaks corresponding to the (220), (311), (400), and (440) planes are observed at 2θ angles of approximately 30°, 35.4°, 43.4°, and 62.7°, respectively (JCPDS card No. 19-0629). These findings further support the presence of Fe3O4 within the synthesized nanoparticles, contributing to the comprehensive understanding of their structural characteristics.

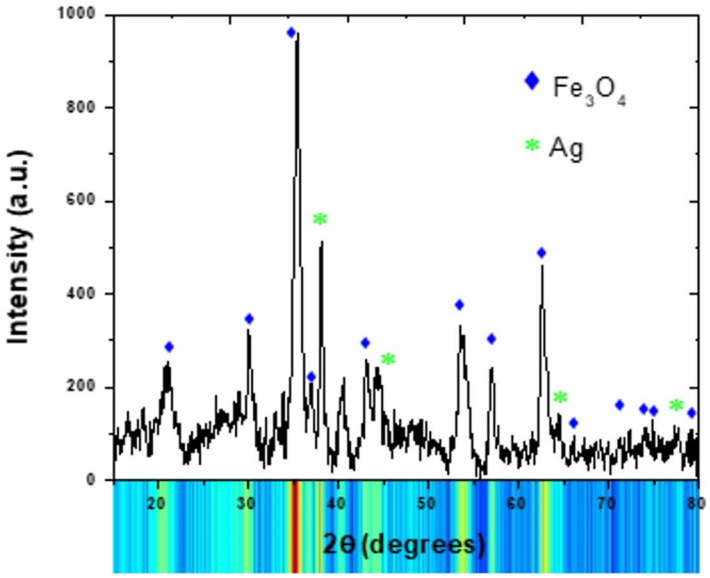

Figure 3. Experimental X-ray Diffraction (XRD) Pattern of the Fe3O4-Ag Decorated Nanoparticles.

3.3. Magnetic Behavior Analysis of Fe3O4/Ag Decorated Nanoparticles

The magnetic behavior of Fe3O4/Ag nanoalloys was comprehensively investigated through hysteresis curve analysis conducted at 300 K (Figure 4a). The obtained hysteresis loops exhibit distinctive characteristics typical of superparamagnetic materials, demonstrating nearly zero magnetic coercivity. Notably, the magnetization value recorded in this plot was determined to be 52 emu/g. This saturation magnetization value can be attributed to several factors, including the presence of non-magnetic surface layers, spin canting phenomena at the surface, or even a surface spin-glass transition[36,37]. In our specific case, the observed phenomenon is plausibly explicable in terms of the chemical bonding of organic molecules, such as polyvinylpyrrolidone (PVP), incorporated into the Fe3O4 nanostructures during the synthesis process, leading to a reduction in the magnetization of the surface layers[38–40].

Furthermore, the magnetization curves exhibit the characteristic blocking process inherent in assemblies of superparamagnetic nanostructures, showcasing a distribution of blocking

 doi:10.20944/preprints202407.0009.v1

temperatures. This behavior is influenced by several factors, including inter-particle distance, size, and shape distribution of particles[41,42]. Such observations are consistent with the behavior typically observed in hybrid materials based on magnetic constituents[43].

The zero-field-cooled (ZFC) curve depicted in Figure 4b displays a broad peak, the maximum of which (TP) is influenced by various factors such as inter-particle distance, size, and shape distribution of particles[37]. Despite the multitude of factors affecting TP, this temperature serves as a rough approximation of the average blocking temperature of the material. This ZFC and field-cooled (FC) behavior aligns with observations seen in other magnetite nanoparticle-based hybrid materials. The broad and flat plateau observed in the ZFC curve can be interpreted within the context of particles exhibiting variations in size and inter-particle distance, further elucidating the complex magnetic behavior of the nanoalloy system[37,44].

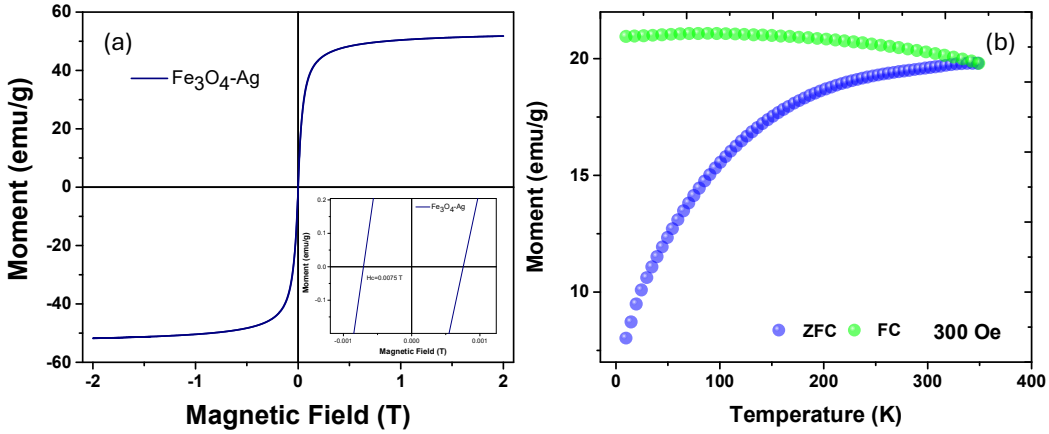

Figure 4. Magnetic Characterization of Fe3O4/Ag Nanoalloys. (a)Hysteresis curve analysis at 300 K confirms superparamagnetic behavior in Fe3O4/Ag nanoalloys, with negligible magnetic coercivity and a magnetization value of 47 emu/g. (b) Zero-field-cooled (ZFC) curve depicts superparamagnetic behavior across temperatures, with a broad peak indicating the average blocking temperature.

3.4. X-ray Photoelectron Spectroscopy (XPS) Analysis

X-ray photoelectron spectroscopy (XPS) analysis was conducted to ascertain the electronic structures or valence states of Fe3O4-Ag nanoalloys. Figure 6(a) depicts the analysis spectra of the Fe3O4-Ag nanostructures. Within these spectra, the signals of Fe 2p, O 1s, and Ag 3d are discernible as principal components of the acquired nanoparticles[45,46]. Figure 5(a) illustrates the Ag 3d region, wherein the Ag d5/2 and Ag d2/3 orbitals are fully identifiable at 368.3 and 374.3 eV, respectively[46], serving as compelling evidence corroborating the presence of Ag as a constituent element of the Fe3O4-Ag nanostructures, as indicated in the preceding characterization results from scanning electron microscopy and energy-dispersive X-ray spectroscopy (EDS).

Additionally, the binding energies of Fe 2p1/2 and Fe 2p3/2 were identified at 724.9 and 711.6 eV, respectively, values associated with the spin–orbit peaks of Fe3O4 (Figure 5b). An energy separation of 13.9 eV between Fe 2p (1/2) and Fe 2p3/2 was observed, a value specifically reported for the core level signal of Fe3O4. Related satellite peaks at 719.4 eV and 733.5 eV were also discerned[47]. Finally, Figure 6(c) reveals a high-resolution X-ray photoelectron spectrum (HRXPS) of the O1(s) orbital, with a binding energy identified at 530.74 eV, associated with the oxygen of Fe3O4. These results collectively serve as evidence of the formation of Fe3O4-Ag nanostructures[48].

 doi:10.20944/preprints202407.0009.v1

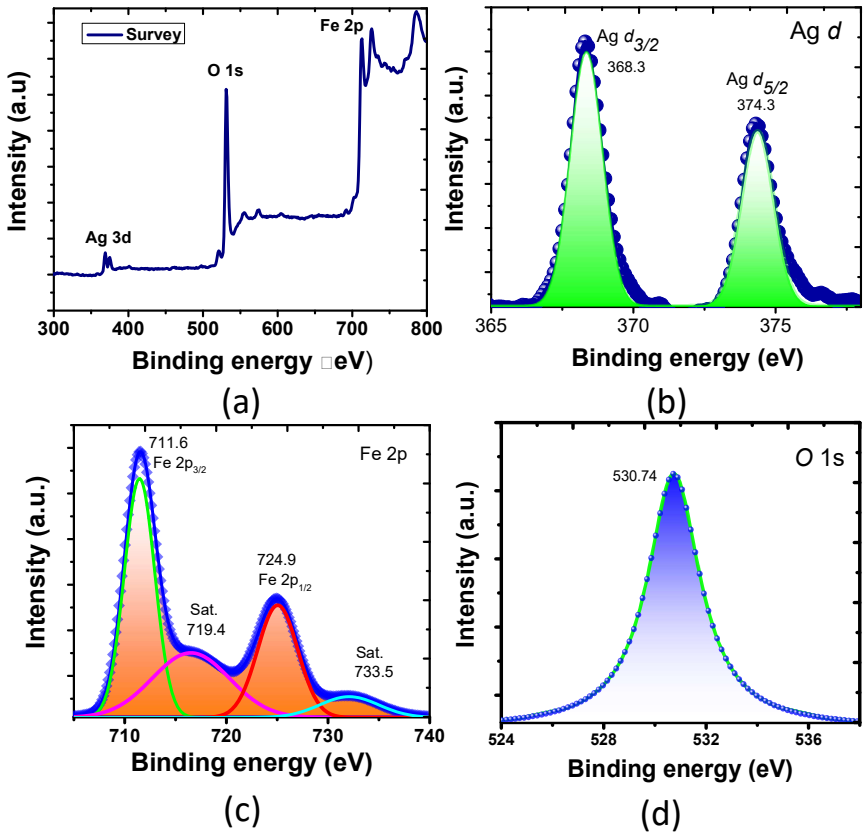

Figure 5. XPS Spectra of Fe3O4-Ag Decorated Nanostructures: (a) Survey Spectra, (b) HR-XPS of Fe 2p, (c) O 1s, and (d) Ag 3d.

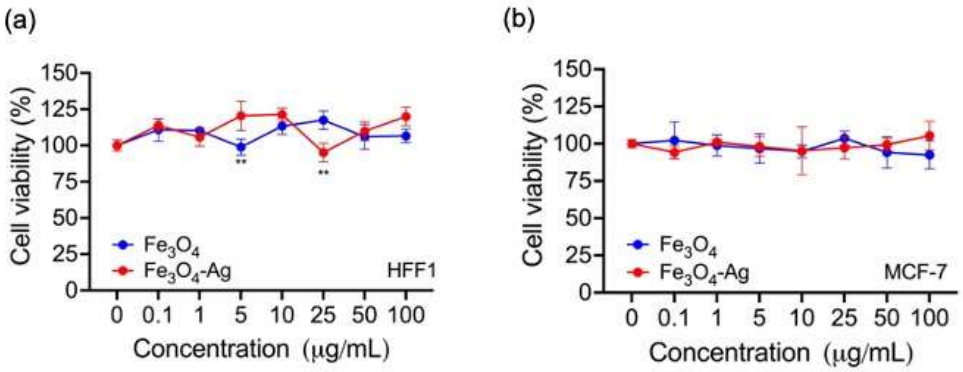

Figure 6. Cell viability assay of Fe_3O_4 and Fe_3O_4-Ag decorated nanoparticles on (a) human fibroblast (HFF-1), and (b) breast cancer (MCF-7) cells. The results of cell viability are expressed as the mean of cell viability percentage ±the standard deviation from three independent experiments. Statistical analysis was performed using two-way ANOVA followed by Tukey's multiple comparison test, significance was indicated as *p<0.05 and **p<0.01.

3.5. Cell Viability of Fe_3O_4 and Fe_3O_4-Ag Decorated Nanoparticles on Human Fibroblast (HFF-1) and Breast Cancer Cells (MCF-7).

To analyze whether the Fe_3O_4 and Fe_3O_4-Ag decorated nanoparticles induce a cytotoxic effect, cell viability test was performed on human fibroblasts and human breast cancer cells. As observed in Figure 6, the cell viability on HFF-1 fibroblast changed across the different concentrations of Fe_3O_4 and Fe_3O_4-Ag decorated nanoparticles. However, none of them reduce significatively the cell viability; thus all the concentrations tested were not cytotoxic. For the other hand, the cell viability of MCF-7 breast cancer cells did not change upon the exposure of cells to different concentrations of

 doi:10.20944/preprints202407.0009.v1

nanoparticles, indicated that all of them are compatible and allowed the cells to growth as in the control.

These results show a clear indication that Fe3O4 and Fe3O4-Ag nanoparticles can be used in some biomedical applications. Additionally, these results have suggested that higher concentrations of Fe3O4 and Fe3O4-Ag nanostructures may be more effective in various applications, potentially due to their selective attack on cancer cells. This higher efficacy at higher concentrations could be attributed to the unique properties and anti-cancer capabilities of these nanoparticles[49,50]. However, it is essential to ensure that these nanoparticles do not exhibit undesirable cytotoxicity towards normal, healthy cells, as this could limit their viability and safety for clinical use[51,52]. Careful evaluation of the effects of nanoparticles on cancerous and non-cancerous cell lines at various concentrations is essential to achieve the appropriate balance between therapeutic efficacy and biocompatibility[53].

3.6. Reactive Oxygen Species (ROS) Induced by Fe_3O_4 and Fe_3O_4-Ag Decorated Nanoparticles on Human Fibroblast (HFF-1) and Breast Cancer Cells (MCF-7)

The production of ROS was measured as showed in Figure 7, to corroborate the biocompatibility of Fe_3O_4 and Fe_3O_4-Ag decorated nanoparticles in human cells. Different concentrations of nanoparticles were tested in human fibroblast cells HFF-1 (Figure 7a), but only higher concentrations (100 µg/mL) of Fe_3O_4-Ag decorated nanoparticles diminished the production of ROS. The same effect was observed in human breast cancer MCF-7 cells as illustrated in Figure 7b, Fe_3O_4-Ag decorated nanoparticles induced a decreased in the level of ROS production only after 50 µg/mL, and at higher concentrations (100 µg/mL) Fe_3O_4 also reduced the level of ROS production.

These findings suggest that Fe3O4-Ag decorated nanoparticles may have a more pronounced effect on modulating oxidative stress in both normal and cancer cells. While Fe3O4 nanoparticles show a greater capacity to generate ROS. Previous studies have shown that the ability of nanoparticles to generate reactive oxygen species is a critical factor in determining their cytotoxicity and potential therapeutic applications[14,54,55]. Enhancing ROS generation may be an effective anticancer strategy, as cancer cells often have higher basal levels of ROS and are more susceptible to further ROS-induced damage. On the other hand, excessive production of ROS can also have detrimental effects on normal cells[55]. The differential response observed between the two cell lines in this study highlights the importance of evaluating the biocompatibility of nanoparticles in cancerous and non-cancerous cells. The findings of this study contribute to the understanding of the interactions between nanoparticles and cellular redox homeostasis, which is crucial for the development of safe and effective nanoparticle-based therapies.

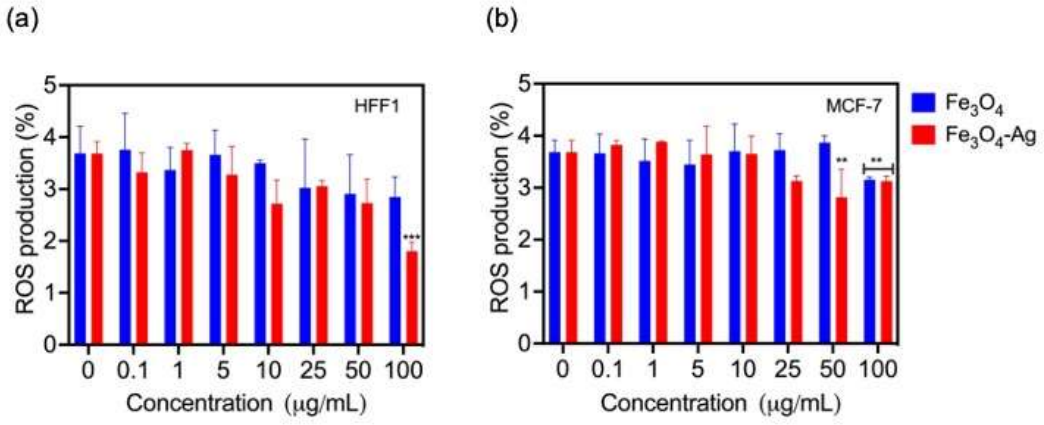

Figure 7. ROS measurement production induced by Fe_3O_4 and Fe_3O_4-Ag decorated nanoparticles on human fibroblast (HFF-1) and breast cancer cells (MCF-7). Statistical analysis was performed using two-way ANOVA followed by Tukey's multiple comparison test. Statistical significance was indicated as *p<0.05 and **p<0.01.

 doi:10.20944/preprints202407.0009.v1

3.7. Hemocompatibility and Nitric Oxide Production Induced by Fe_3O_4 and Fe_3O_4-Ag Decorated Nanoparticles

To ensure the biocompatibility of both Fe_3O_4 and Fe_3O_4-Ag decorated nanoparticles, a hemolysis assay was conducted on human red blood cells. The threshold for hemocompatibility is indicated by the dotted black line at 5% of hemolysis. According to this criterion, all concentrations below 25 µg/mL of both types of nanoparticles were hemocompatible, as the percentage of red blood cell lysis remained below 5%. However, concentrations of 50 and 100 µg/mL of Fe_3O_4 and Fe_3O_4-Ag decorated nanoparticles clearly induced erythrocyte lysis, thus proving toxic to these cells.

To determine whether Fe_3O_4 and Fe_3O_4-Ag decorated nanoparticles induce an *in vitro* inflammatory response, nitrite production was measured upon the exposure of macrophages to different concentrations of nanoparticles. As illustrated in Figure 8b, concentrations below 10 µg/mL of both type of nanoparticles induced small concentrations of nitrites (less than 20 µM). However, concentrations above 25 µg/mL of Fe_3O_4 and Fe_3O_4-Ag decorated nanoparticles clearly induced higher amounts of nitrites (30 to 42 µM), eliciting an inflammatory *in vitro* response comparable to the control, where the nitrites concentration is 50 µM.

These findings suggest that Fe3O4 and Fe3O4-Ag decorated nanoparticles exhibit promising hemocompatibility and low inflammatory potential at concentrations below 25 µg/mL, making them potentially suitable candidates for various biomedical applications[6]. The observed hemocompatibility, where the percentage of red blood cell synthesis remained below the 5% threshold, indicates that these nanoparticles are unlikely to cause significant damage to erythrocytes at lower concentrations. Similarly, the relatively low levels of nitrite production, a marker of inflammation, suggest that these nanoparticles elicit a minimal inflammatory response in macrophages at lower doses. However, the study also revealed that higher concentrations of 50 and 100 µg/mL of decorated Fe3O4 and Fe3O4-Ag nanoparticles can induce significant erythrocyte synthesis and higher levels of nitrite, suggesting potential toxicity and a more pronounced inflammatory reaction. This highlights the importance of carefully considering the dosage and design of these nanoparticles to ensure their safe and effective use in biomedical contexts[56,57]. Further optimization and comprehensive evaluation of their biocompatibility at different concentrations will be crucial to develop these nanoparticles as reliable and safe tools for various therapeutic and diagnostic applications[58].

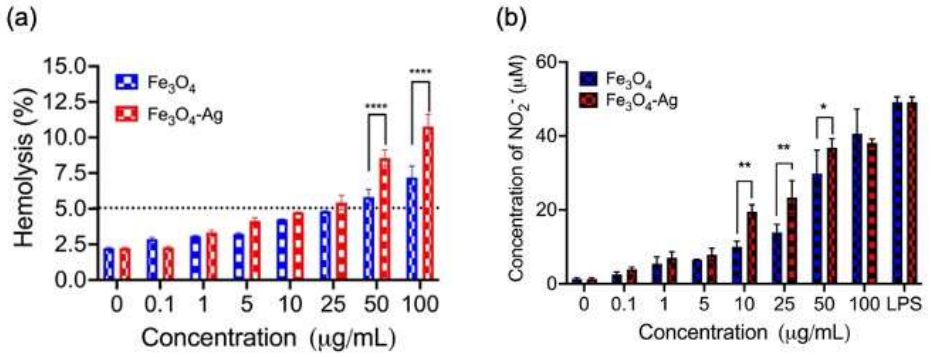

Figure 8. (a) Hemolysis of erythrocytes and (b) nitrite production in macrophages induced by Fe_3O_4 and Fe_3O_4-Ag decorated nanoparticles. Statistical analysis was performed using two-way ANOVA followed by Tukey's multiple comparison test. Statistical significance was indicated as *p<0.05, **p<0.01, and *** p>0.001.

5. Conclusions.

The study analyzed the cytotoxic effects of Fe3O4 and Fe3O4-Ag decorated nanoparticles on human fibroblasts (HFF-1) and breast cancer cells (MCF-7) to evaluate their biocompatibility and potential therapeutic efficacy. The results showed that neither type of nanoparticle significantly

reduced cell viability in HFF-1 fibroblasts, indicating that they are non-cytotoxic at the tested concentrations. Similarly, MCF-7 breast cancer cells did not exhibit a significant change in viability when exposed to different nanoparticle concentrations, suggesting that these nanoparticles are biocompatible and allow normal cell growth. This highlights the potential of Fe3O4 and Fe3O4-Ag nanoparticles for biomedical applications, given their compatibility with both healthy and cancerous cells.

The production of reactive oxygen species (ROS) by Fe3O4 and Fe3O4-Ag nanoparticles was also examined to further assess their biocompatibility and therapeutic potential. The study found that higher concentrations of Fe3O4-Ag nanoparticles decreased ROS production in both HFF-1 and MCF-7 cells, while Fe3O4 nanoparticles were more effective in generating ROS at these concentrations. This differential response indicates that Fe3O4-Ag nanoparticles might modulate oxidative stress more effectively, which could be beneficial for anticancer strategies due to the susceptibility of cancer cells to ROS-induced damage. However, excessive ROS production can harm normal cells, underscoring the need for careful evaluation of nanoparticle concentrations to balance therapeutic efficacy and safety. These findings contribute to the understanding of nanoparticle interactions with cellular oxidative mechanisms, crucial for developing safe and effective nanoparticle-based therapies.

Author Contributions: Conceptualization, A.D.J.RB. and K.J.M.; methodology, K.J.M., S.Y.R.L and A.J.R.B; software, K.J.M. and A.D.J.R.B.; validation, K.J.M.; formal analysis, K.J.M. and A.J.R.B.; investigation, K.J.M. and A.D.J.R.B.; resources, A.D.J.R.B and K.J.M.; data curation, K.J.M and A.D.J.RB.; writing—original draft preparation, A.D.J.RB. and K.J.M; writing—review and editing, K.J.M, A.D.J.RB., NML and SYRL.; visualization, K.J.M, A.D.J.RB., S.Y.R.L. and N.M.L.; supervision, K.J.M and A.D.J.RB.; project administration, A.D.J.R.B.; funding acquisition, A.D.J.RB., S.Y.R.L., N.M.L. and K.J.M.

Acknowledgments: Álvaro de Jesús Ruíz-Baltazar wishes to express profound gratitude for the invaluable support provided by the National Council for Humanities, Science, and Technology (CONAHCYT, Mexico), in collaboration with the Center of Applied Physics and Advanced Technology (CFATA-UNAM), through the "Investigadoras e Investigadores por México-CONAHCYT" program. Additionally, heartfelt thanks are extended to the "Instituto de Ciencias Biomédicas de la UACJ" for their unwavering support during the sabbatical period. The authors would like to express their gratitude and acknowledge the unconditional support provided by NanoToxLab, part of CFATA-UNAM, in the realization of this research. Additionally, the authors appreciate the support from the Microscopy Laboratory at the National Laboratory for Materials Characterization (LanCam), through the academic technician Manuel Aguilar Franco.

Conflicts of Interest: The authors declare no conflicts of interest.

References

1. Kumar, A.; Shah, S.R.; Jayeoye, T.J.; Kumar, A.; Parihar, A.; Prajapati, B.; Singh, S.; Kapoor, D.U. Biogenic Metallic Nanoparticles: Biomedical, Analytical, Food Preservation, and Applications in Other Consumable Products. *Frontiers in Nanotechnology* 2023, *5*.
2. Krishnasamy, R.; Obbineni, J.M. Methods for Green Synthesis of Metallic Nanoparticles Using Plant Extracts and Their Biological Applications-A Review. *Journal of Biomimetics, Biomaterials and Biomedical Engineering* **2022**, *56*, doi:10.4028/p-8bf786.
3. Yaraki, M.T.; Zahed Nasab, S.; Zare, I.; Dahri, M.; Moein Sadeghi, M.; Koohi, M.; Tan, Y.N. Biomimetic Metallic Nanostructures for Biomedical Applications, Catalysis, and Beyond. *Ind Eng Chem Res* 2022, *61*.
4. Antonelli, A.; Magnani, M. SPIO Nanoparticles and Magnetic Erythrocytes as Contrast Agents for Biomedical and Diagnostic Applications. *J Magn Magn Mater* **2022**, *541*, doi:10.1016/j.jmmm.2021.168520.
5. Antonelli, A.; Magnani, M. SPIO Nanoparticles and Magnetic Erythrocytes as Contrast Agents for Biomedical and Diagnostic Applications. *J Magn Magn Mater* **2022**, *541*, doi:10.1016/j.jmmm.2021.168520.
6. Materón, E.M.; Miyazaki, C.M.; Carr, O.; Joshi, N.; Picciani, P.H.S.; Dalmaschio, C.J.; Davis, F.; Shimizu, F.M. Magnetic Nanoparticles in Biomedical Applications: A Review. *Applied Surface Science Advances* **2021**, *6*, doi:10.1016/j.apsadv.2021.100163.
7. Liu, X.; Wang, X.; Zhang, H.; Li, X.; Wang, Y.; Zhang, X. Magnetoplasmonic Materials for Biomedical Applications: Synthesis and Properties. *J Mater Chem B* **2019**, *7*, 1917–1930.
8. Klein, S.; Hübner, J.; Menter, C.; Distel, L.V.R.; Neuhuber, W.; Kryschi, C. A Facile One-Pot Synthesis Ofwater-Soluble, Patchy Fe3O4-Au Nanoparticles for Application in Radiation Therapy. *Applied Sciences (Switzerland)* **2019**, *9*, doi:10.3390/app9010015.

9. Danafar, H.; Baghdadchi, Y.; Barsbay, M.; Ghaffarlou, M.; Mousazadeh, N.; Mohammadi, A. Synthesis of Fe3O4-Gold Hybrid Nanoparticles Coated by Bovine Serum Albumin as a Contrast Agent in MR Imaging. *Heliyon* **2023**, *9*, e13874–e13874, doi:https://doi.org/10.1016/j.heliyon.2023.e13874.
10. de Jesús Ruíz-Baltazar, Á. Green Synthesis Assisted by Sonochemical Activation of Fe3O4-Ag Nano-Alloys: Structural Characterization and Studies of Sorption of Cationic Dyes. *Inorg Chem Commun* **2020**, *120*, 108148, doi:https://doi.org/10.1016/j.inoche.2020.108148.
11. Alshameri, A.W.; Owais, M. Antibacterial and Cytotoxic Potency of the Plant-Mediated Synthesis of Metallic Nanoparticles Ag NPs and ZnO NPs: A Review. *OpenNano* **2022**, *8*, 100077, doi:https://doi.org/10.1016/j.onano.2022.100077.
12. Sarani, M.; Roostaee, M.; Adeli-Sardou, M.; Kalantar-Neyestanaki, D.; Mousavi, S.A.A.; Amanizadeh, A.; Barani, M.; Amirbeigi, A. Green Synthesis of Ag and Cu-Doped Bismuth Oxide Nanoparticles: Revealing Synergistic Antimicrobial and Selective Cytotoxic Potentials for Biomedical Advancements. *Journal of Trace Elements in Medicine and Biology* **2024**, *81*, 127325, doi:https://doi.org/10.1016/j.jtemb.2023.127325.
13. Pannerselvam, B.; Thiyagarajan, D.; Pazhani, A.; Thangavelu, K.P.; Kim, H.J.; Rangarajulu, S.K. Copperpod Plant Synthesized Agnps Enhance Cytotoxic and Apoptotic Effect in Cancer Cell Lines. *Processes* **2021**, *9*, doi:10.3390/pr9050888.
14. Swathi, S.; Ameen, F.; Ravi, G.; Yuvakkumar, R.; Hong, S.I.; Velauthapillai, D.; AlKahtani, M.D.F.; Thambidurai, M.; Dang, C. Cancer Targeting Potential of Bioinspired Chain like Magnetite (Fe3O4) Nanostructures. *Current Applied Physics* **2020**, *20*, 982–987, doi:10.1016/j.cap.2020.06.013.
15. Mukha, I.; Chepurna, O.; Vityuk, N.; Khodko, A.; Storozhuk, L.; Dzhagan, V.; Zahn, D.R.T.; Ntziachristos, V.; Chmyrov, A.; Ohulchanskyy, T.Y. Multifunctional Magneto-Plasmonic Fe3o4/Au Nanocomposites: Approaching Magnetophoretically-Enhanced Photothermal Therapy. *Nanomaterials* **2021**, *11*, doi:10.3390/nano11051113.
16. Usman, F.; Ghazali, K.H.; Muda, R.; Johari, N.H.; Dennis, J.O.; Tamam, N.; Sulieman, A.; Ji, Y. Magnetoresistance and Magneto-Plasmonic Sensors for the Detection of Cancer Biomarkers: A Bibliometric Analysis and Recent Advances. *Sensors and Actuators Reports* **2023**, *6*, 100172, doi:https://doi.org/10.1016/j.snr.2023.100172.
17. Singh, R.S.; Sarswat, P.K. From Fundamentals to Applications: The Development of Magnetoplasmonics for next-Generation Technologies. *Materials Today Electronics* **2023**, *4*, 100033, doi:10.1016/j.mtelec.2023.100033.
18. Raja, K.; Balamurugan, V.; Selvakumar, S.; Vasanth, K. Striga Angustifolia Mediated Synthesis of Silver Nanoparticles: Anti-Microbial, Antioxidant and Anti-Proliferative Activity in Apoptotic P53 Signalling Pathway. *J Drug Deliv Sci Technol* **2022**, *67*, 102945, doi:https://doi.org/10.1016/j.jddst.2021.102945.
19. Enciu, A.-M.; Codrici, E.; Popescu, D.I.; Preda, P.; Stan, D.; Avram, M.; Tanase, C. Aloe Vera Gel and Sea-Buckthorn Oil Protect Human Fibroblasts against Silver Nanoparticles Cytotoxicity. *Toxicol Lett* **2021**, *350*, S238–S239, doi:https://doi.org/10.1016/S0378-4274(21)00793-1.
20. Lewinska, A.; Adamczyk-Grochala, J.; Bloniarz, D.; Olszowka, J.; Kulpa-Greszta, M.; Litwinienko, G.; Tomaszewska, A.; Wnuk, M.; Pazik, R. AMPK-Mediated Senolytic and Senostatic Activity of Quercetin Surface Functionalized Fe3O4 Nanoparticles during Oxidant-Induced Senescence in Human Fibroblasts. *Redox Biol* **2020**, *28*, 101337, doi:https://doi.org/10.1016/j.redox.2019.101337.
21. undefined undefined; undefined undefined; undefined undefined; undefined undefined; undefined undefined; undefined undefined; undefined undefined Metallodrugs against Breast Cancer: Combining the Tamoxifen Vector with Platinum(II) and Palladium(II) Complexes. **2023**.
22. Singh, R.S.; Sarswat, P.K. From Fundamentals to Applications: The Development of Magnetoplasmonics for next-Generation Technologies. *Materials Today Electronics* **2023**, *4*, 100033, doi:https://doi.org/10.1016/j.mtelec.2023.100033.
23. Liu, X.; Wang, X.; Zhang, H.; Li, X.; Wang, Y.; Zhang, X. Magnetoplasmonic Nanomaterials for Biomedical Applications. *Nanoscale Adv* **2020**, *2*, 2524–2540.
24. Liu, X.; Wang, X.; Zhang, H.; Li, X.; Wang, Y.; Zhang, X. Magnetoplasmonic Nanomaterials for Biosensing and Bioimaging Applications. *J Mater Chem B* **2021**, *9*, 4688–4708.
25. Jandrotia, R.; Gupta, I.; Mahajan, P.; Batish, D.R.; Singh, H.P. 2 - Green Nanomaterials: An Eco-Friendly Route for Sustainable Nanotechnology. In *Nanotechnology and Nanomaterials in the Agri-Food Industries*; Singh, P., Khare, P., Mishra, D., Bilal, M., Sillanpää, M., Eds.; Micro and Nano Technologies; Elsevier, 2024; pp. 21–52 ISBN 978-0-323-99682-2.
26. Rahmayanti, M.; Nurul Syakina, A.; Fatimah, I.; Sulistyaningsih, T. Green Synthesis of Magnetite Nanoparticles Using Peel Extract of Jengkol (Archidendron Pauciflorum) for Methylene Blue Adsorption from Aqueous Media. *Chem Phys Lett* **2022**, *803*, 139834, doi:10.1016/j.cplett.2022.139834.
27. Zhang, X.F.; Liu, Z.G.; Shen, W.; Gurunathan, S. Silver Nanoparticles: Synthesis, Characterization, Properties, Applications, and Therapeutic Approaches. *Int J Mol Sci* 2016, *17*.
28. Cheng, Z.; Tang, S.W.; Feng, J.; Wu, Y. Biosynthesis and Antibacterial Activity of Silver Nanoparticles Using Flos Sophorae Immaturus Extract. *Heliyon* **2022**, *8*, doi:10.1016/j.heliyon.2022.e10010.

29. Kobylinska, N.; Klymchuk, D.; Khaynakova, O.; Duplij, V.; Matvieieva, N. Morphology-Controlled Green Synthesis of Magnetic Nanoparticles Using Extracts of 'Hairy' Roots: Environmental Application and Toxicity Evaluation. *Nanomaterials* **2022**, *12*, doi:10.3390/nano12234231.
30. Antwi-Baah, R.; Wang, Y.; Chen, X.; Liu, H.; Yu, K. Hybrid Morphologies of Paramagnetic Manganese-Based Nanoparticles as Theranostics. *Chemical Engineering Journal* **2023**, *466*, 142970, doi:https://doi.org/10.1016/j.cej.2023.142970.
31. Sánchez-López, E.; Gomes, D.; Esteruelas, G.; Bonilla, L.; Lopez-Machado, A.L.; Galindo, R.; Cano, A.; Espina, M.; Ettcheto, M.; Camins, A.; et al. Metal-Based Nanoparticles as Antimicrobial Agents: An Overview. *Nanomaterials* 2020, *10*.
32. Kansız, S.; Elçin, Y.M. Advanced Liposome and Polymersome-Based Drug Delivery Systems: Considerations for Physicochemical Properties, Targeting Strategies and Stimuli-Sensitive Approaches. *Adv Colloid Interface Sci* **2023**, *317*, 102930, doi:https://doi.org/10.1016/j.cis.2023.102930.
33. Nair, V. V; Cabrera, P.; Ramírez-Lecaros, C.; Jara, M.O.; Brayden, D.J.; Morales, J.O. Buccal Delivery of Small Molecules and Biologics: Of Mucoadhesive Polymers, Films, and Nanoparticles – An Update. *Int J Pharm* **2023**, *636*, 122789, doi:https://doi.org/10.1016/j.ijpharm.2023.122789.
34. Pérez-Díaz, M.; Alvarado-Gomez, E.; Magaña-Aquino, M.; Sánchez-Sánchez, R.; Velasquillo, C.; Gonzalez, C.; Ganem-Rondero, A.; Martínez-Castañon, G.; Zavala-Alonso, N.; Martinez-Gutierrez, F. Anti-Biofilm Activity of Chitosan Gels Formulated with Silver Nanoparticles and Their Cytotoxic Effect on Human Fibroblasts. *Materials Science and Engineering: C* **2016**, *60*, 317–323, doi:https://doi.org/10.1016/j.msec.2015.11.036.
35. Itoo, A.M.; Vemula, S.L.; Gupta, M.T.; Giram, M.V.; Kumar, S.A.; Ghosh, B.; Biswas, S. Multifunctional Graphene Oxide Nanoparticles for Drug Delivery in Cancer. *Journal of Controlled Release* **2022**, *350*, 26–59, doi:https://doi.org/10.1016/j.jconrel.2022.08.011.
36. Salih, S.J.; Mahmood, W.M. Review on Magnetic Spinel Ferrite (MFe2O4) Nanoparticles: From Synthesis to Application. *Heliyon* **2023**, *9*, e16601, doi:https://doi.org/10.1016/j.heliyon.2023.e16601.
37. Espinosa, A.; Reguera, J.; Curcio, A.; Muñoz-Noval, Á.; Kuttner, C.; Van de Walle, A.; Liz-Marzán, L.M.; Wilhelm, C. Janus Magnetic-Plasmonic Nanoparticles for Magnetically Guided and Thermally Activated Cancer Therapy. *Small* **2020**, *16*, doi:10.1002/smll.201904960.
38. Hong, T.; Jiang, M.; Hu, Y.; Tang, Z.; Huang, K. Nonlinear Magnetization Relaxation of Uniaxial Anisotropic Ferromagnetic Particles with Linear Reaction Dynamics Driven by a Strong Ac Magnetic Field. *Chem Phys Lett* **2021**, *782*, 139017, doi:10.1016/j.cplett.2021.139017.
39. Bôa Morte, E.F.; Marum, D.S.; Saitovitch, E.B.; Alzamora, M.; Monteiro, S.N.; Sanchez Rodriguez, R.J. Modified Magnetite Nanoparticle as Biocatalytic Support for Magnetically Stabilized Fluidized Bed Reactors. *Journal of Materials Research and Technology* **2021**, *14*, 1112–1125, doi:10.1016/j.jmrt.2021.06.105.
40. Lai, C.-H.; Chuang, Y.-K.; Chang, Y.-C.; Chen, C.-H.; Chen, P.-Y.; Chen, I.-W.; Chen, Y.-C. Magnetic-Plasmonic Core-Shell Nanoparticles for Multimodal Biomedical Imaging. *Nanotechnology* **2017**, *28*, 135102, doi:10.1088/1361-6528/aa5d6f.
41. Tan, L.K.S.; How, C.W.; Low, L.E.; Ong, B.H.; Loh, J.S.; Lim, S.-Y.; Ong, Y.S.; Foo, J.B. Magnetic-Guided Targeted Delivery of Zerumbone/SPION Co-Loaded in Nanostructured Lipid Carrier into Breast Cancer Cells. *J Drug Deliv Sci Technol* **2023**, *87*, 104830, doi:https://doi.org/10.1016/j.jddst.2023.104830.
42. Korolkov, I. V; Shumskaya, A.; Kozlovskiy, A.L.; Kaliyekperov, M.E.; Lissovskaya, L.I.; Zdorovets, M. V Magnetic-Plasmonic Ni Nanotubes Covered with Gold for Improvement of SERS Analysis. *J Alloys Compd* **2022**, *901*, 163661, doi:https://doi.org/10.1016/j.jallcom.2022.163661.
43. Garanina, A.S.; Efremova, M. V.; Machulkin, A.E.; Lyubin, E. V.; Vorobyeva, N.S.; Zhironkina, O.A.; Strelkova, O.S.; Kireev, I.I.; Alieva, I.B.; Uzbekov, R.E.; et al. Bifunctional Magnetite–Gold Nanoparticles for Magneto-Mechanical Actuation and Cancer Cell Destruction. *Magnetochemistry* **2022**, *8*, doi:10.3390/magnetochemistry8120185.
44. Magnetic-Plasmonic Nanoparticles for the Life Sciences: Calculated ...
45. de Jesús Ruíz-Baltazar, Á. Sonochemical Activation-Assisted Biosynthesis of Au/Fe3O4 Nanoparticles and Sonocatalytic Degradation of Methyl Orange. *Ultrason Sonochem* **2021**, *73*, 105521, doi:https://doi.org/10.1016/j.ultsonch.2021.105521.
46. Amarjargal, A.; Tijing, L.D.; Im, I.T.; Kim, C.S. Simultaneous Preparation of Ag/Fe3O4 Core-Shell Nanocomposites with Enhanced Magnetic Moment and Strong Antibacterial and Catalytic Properties. *Chemical Engineering Journal* **2013**, *226*, 243–254, doi:10.1016/j.cej.2013.04.054.
47. Pieretti, J.C.; Gonçalves, M.C.; Nakazato, G.; Santos de Souza, A.C.; Boudier, A.; Seabra, A.B. Multifunctional Hybrid Nanoplatform Based on Fe3O4@Ag NPs for Nitric Oxide Delivery: Development, Characterization, Therapeutic Efficacy, and Hemocompatibility. *J Mater Sci Mater Med* **2021**, *32*, doi:10.1007/s10856-021-06494-x.
48. Nguyen, M.D.; Tran, H.V.; Xu, S.; Lee, T.R. Fe3O4 Nanoparticles: Structures, Synthesis, Magnetic Properties, Surface Functionalization, and Emerging Applications. *Applied Sciences (Switzerland)* 2021, *11*.

49. Siddique, S.; Chow, J.C.L. Application of Nanomaterials in Biomedical Imaging and Cancer Therapy. *Nanomaterials* 2020, *10*, 1–41.
50. Kumar, V.; Kaushik, N.K.; Tiwari, S.K.; Singh, D.; Singh, B. Green Synthesis of Iron Nanoparticles: Sources and Multifarious Biotechnological Applications. *Int J Biol Macromol* 2023, *253*.
51. Upadhyay, K.; Tamrakar, R.K.; Thomas, S.; Kumar, M. Surface Functionalized Nanoparticles: A Boon to Biomedical Science. *Chem Biol Interact* 2023, *380*.
52. Khanna, N.; Chatterji, T.; Singh, S.; Pandey, S. Application of Stimuli Responsive Nanocomposites in Drug Delivery and Theranostics to Counter Cancer Proliferation and Drug Resistance. *J Drug Deliv Sci Technol* 2023, *88*.
53. Anderson, J.M. Future Challenges in the in Vitro and in Vivo Evaluation of Biomaterial Biocompatibility. *Regen Biomater* 2016, *3*, 73–77.
54. Yang, L.X.; Wu, Y.N.; Wang, P.W.; Huang, K.J.; Su, W.C.; Shieh, D. Bin Silver-Coated Zero-Valent Iron Nanoparticles Enhance Cancer Therapy in Mice through Lysosome-Dependent Dual Programed Cell Death Pathways: Triggering Simultaneous Apoptosis and Autophagy Only in Cancerous Cells. *J Mater Chem B* **2020**, *8*, 4122–4131, doi:10.1039/c9tb01477b.
55. Sankaranarayanan, S.A.; Thomas, A.; Revi, N.; Ramakrishna, B.; Rengan, A.K. Iron Oxide Nanoparticles for Theranostic Applications - Recent Advances. *J Drug Deliv Sci Technol* 2022, *70*.
56. Siddiqui, M.A.; Wahab, R.; Saquib, Q.; Ahmad, J.; Farshori, N.N.; Al-Sheddi, E.S.; Al-Oqail, M.M.; Al-Massarani, S.M.; Al-Khedhairy, A.A. Iron Oxide Nanoparticles Induced Cytotoxicity, Oxidative Stress, Cell Cycle Arrest, and DNA Damage in Human Umbilical Vein Endothelial Cells. *Journal of Trace Elements in Medicine and Biology* **2023**, *80*, doi:10.1016/j.jtemb.2023.127302.
57. Krishnan, N.; Peng, F.X.; Mohapatra, A.; Fang, R.H.; Zhang, L. Genetically Engineered Cellular Nanoparticles for Biomedical Applications. *Biomaterials* 2023, *296*.
58. Joshi, R.; Missong, H.; Mishra, J.; Kaur, S.; Saini, S.; Kandimalla, R.; Reddy, P.H.; Babu, A.; Bhatti, G.K.; Bhatti, J.S. Nanotheranostics Revolutionizing Neurodegenerative Diseases: From Precision Diagnosis to Targeted Therapies. *J Drug Deliv Sci Technol* 2023, *89*.